Sun, X. C., Kawashita, L. F., Kaddour, A. S., Hiley, M. J., & Hallett, S. R. (2018). Comparison of low velocity impact modelling techniques for thermoplastic and thermoset polymer composites. *Composite Structures*, *203*, 659-671. https://doi.org/10.1016/j.compstruct.2018.07.054

Comparison of Low Velocity Impact Modelling Techniques for Thermoplastic and Thermoset Polymer Composites

XC. Sun [*a], LF. Kawashita [a], AS. Kaddour [b], MJ. Hiley [b], SR. Hallett [a]

[a] Bristol Composite Institute (ACCIS), University of Bristol, Queen's Building, University Walk Bristol, BS8 1TR, UK
[b] Air and Space Division, QinetiQ, Ively Road, Farnborough, GU14 0LX, UK.

Abstract

This paper presents comparisons between experimental and numerical studies of low-velocity impact damage for thermoplastic (IM7/PEEK) and thermoset (IMS65/MTM) carbon fibre reinforced composites. The experiments were conducted at two key impact energies (8 and 30J) under identical conditions allowing a systematic comparison to be made. Three LS-dyna Finite Element Analysis (FEA) models (standard, continuum damage mechanics (CDM) and discrete) were implemented, all using cohesive interface elements for delamination. The role of Mode II fracture toughness is highlighted. The predictive capabilities of different modelling techniques are compared and discussed and the CDM model gave better correlation with experiments. Fibre failure was predicted by the numerical approaches. The thermoplastic materials did not show noticeably superior behaviour to the thermoset materials and were governed by unstable delamination damage propagation for the same impact energy.

Keywords: Thermoplastic; Thermoset; Composite; Low-velocity impact; Finite Element Analysis (FEA)

[*] Author to whom correspondence should be addressed. Email: ric.sun@bristol.ac.uk

1. INTRODUCTION

It is well known that low velocity impact on composites structures, such as that caused by runway debris during aircraft take-off and landing and dropped tools, can lead to damage in the form of matrix cracking, delaminations and even fibre damage. As some of the damage modes can have detrimental effects on the residual strength, a great deal of attention has been given and remains the focus of interest by the design community regarding the susceptibility of laminated composites to undesirable damage development, resulting from delamination, matrix cracking and fibre failure. A thorough understanding of the response to low velocity impact of composites structures in industrial applications is, therefore, one of the major challenges in demonstrating reliable and safe design.

Methods of reducing the amount of delamination in composites are numerous and one example is the use of toughened matrix systems. The most commonly used systems are thermoset (i.e. epoxy) matrices and thermoplastic (e.g. Polyether ether ketone, known as PEEK). PEEK has been shown by a number of researchers and suppliers to have a relatively higher fracture toughness and strength than conventional epoxy resins and is expected to exhibit better impact resistance and impact damage tolerance [**Error! Reference source not found.**]. Little attention has been given to research related to the damage behaviour and mechanisms under low-velocity impact of PEEK composites.

Thermoplastics have generally been used in secondary or tertiary components (e.g. cleats) whereas epoxy composites are used in primary structures [**Error! Reference source not found.**]. Nonetheless, PEEK composites have seen a renewed interest in recent years, particularly due to their fast processing times and recyclability [**Error! Reference source not found.**] and the introduction of new fibres. It is therefore important to establish the confidence and understand the differences between these two composites both experimentally and numerically through reliable simulations.

Little, and often confusing, information is available in the literature concerning experimental investigations of true comparison between various material systems for the same geometry and impact parameters. Some investigations have shown that PEEK based carbon composites exhibited less damage tolerant than epoxy-based carbon composites [1,6,53]. Chou et al [1] described UT500/PEEK and AS4/PEEK as a ‘non-compatible’ type, which is defined as materials having poor impact resistance under low velocities even though their Model II delamination resistance was quoted to be superior. Morita et al [**Error! Reference source not found.**] examined the impact resistance of AS4/PEEK and a toughened T800/3900 epoxy system under low and high velocity. They observed that AS4/PEEK had a lower impact resistance than T800/3900 in both low and high velocity impact cases. In contrast, other

investigations [**Error! Reference source not found.**] have shown that PEEK based composites have superior impact damage tolerance. Dorey et al [**Error! Reference source not found.**] and Bishop [**Error! Reference source not found.**] demonstrated a clear advantages of PEEK composites over epoxy composites under low-velocity impact (< 10 J) and showed post-impact (5 J) to have severe surface indentation and damage but much less extensive splitting at the back face than carbon/epoxy.

Those inconsistent observational results from the literature remain a challenging hurdle as they give a rise to some concerns over which material performs best at given conditions. This represents the impetus for the present work.

Various numerical studies have been conducted to understand low-velocity impact damage of composite, mainly using Finite Element Analysis (FEA) [8-**Error! Reference source not found.**] with sophisticated material models, such as 'Continuum Damage Mechanics' (CDM) and 'discrete' methods. CDM uses either stress- or strain-based criterion for damage initiations, after which the material stiffnesses are degraded by monotonic increasing damage variables to simulate damage propagations. A number of investigators (e.g. [**Error! Reference source not found.**]) have demonstrated the power of a three dimensional (3D) material model, together with Cohesive Zone Modelling (CZM) approach for the prediction of interlaminar damage under low-velocity impact. Others [**Error! Reference source not found.**] used similar CDM based approach to model ply damage and proposed a way to approximate delamination using modified cohesive crack models with a crack density parameter.

The other approach for modelling intraply damage is based on a discrete approach in which the fibre failure is simply controlled by stress or strain or a statistically based criterion. This approach has been frequently used to investigate the tensile failure of laminated composites with and without holes [24-27]. Cohesive elements are usually inserted between elements of a ply to model matrix cracks, which together with the fibre damage criterion have proved to provide similar modelling capabilities at the ply level to fully damageable 3D CDM models [**Error! Reference source not found.**]. In the discrete approaches, elements with 'zero' stiffness are usually deleted after being completely failed in the simulation, which makes them detectable as clear damage 'band', occasionally captured in experiments. Elements with the same state governed by CDM methods normally are kept in the analysis, giving a continuous damage zone. As the aforementioned post-impact observations of Carbon/PEEK [2], it was expected that the CDM model is preferable for modelling Carbon/PEEK in the sense of the material's post-damage behaviour, and vice versa for discrete approach and Carbon/epoxy. It

can be concluded from above that questions, as to which modelling approach is the most suitable for predicting which material system, have not been fully answered in the literature.

In the current paper, low-velocity impact response and damage behaviour of both Carbon/PEEK and Carbon/epoxy were investigated experimentally and numerically under unified conditions. FEA was conducted using a CDM approach based on a material model from [**Error! Reference source not found.**] and Weibull theory predicting ply damage [27], and a CZM material model [**Error! Reference source not found.**] for capturing delamination, to simulate the impact event and damage. This paper is focused on a systematic comparison between three LS-Dyna material models and their application and correlations with test results on epoxy- and PEEK-based composites material systems, having the same thickness and lay-ups.

2. EXPERIMENT

Two carbon fibre material systems were considered in this study: IMS65 fibre with out-of-autoclave epoxy MTM44-1 (designated as IMS65/MTM in the remainder of this paper) and IM7 fibre with PEEK thermoplastic resin (designated as IM7/PEEK). Both types of laminate were fabricated by 32 plies with stacking sequence of $[0/90/+45/-45_2/+45/90/0]_{2S}$. The nominal ply and overall thickness were 0.125 mm and 4 mm, respectively for both material types. The material properties are listed in Table 1. All impact tests were performed using an Imatek IM10 drop-weight impact tower fitted with a 16 mm diameter hemispherical tup. The latter was 3.87 kg in mass and was instrumented enabling force/time and force/deflection data to be collected. Panels were fully clamped and sandwiched by two steel rings with 100 mm internal diameter. Two impact energies of 8 J and 30 J were used for both laminates, with 3 specimens used per energy level. The post-impact specimens were examined using QinetiQ's Non-Destructive Testing (NDT) techniques such as ultrasonic C-scan and X-ray Computational Tomographic (CT) scan, to determine the damage behaviour.

3. NUMERICAL MODELLING

3.1 Model Descriptions

Commercial software LS-Dyna was used to carry out FE analysis in this paper. Interface layers of cohesive elements, 0.01 mm thick, were inserted between plies with different fibre orientations (no delamination was observed between plies with the same fibre orientation [**Error! Reference source not found.**]). By blocking plies with the same fibre orientations, the 32 plies were reduced to 25 ply-blocks with 24 layers in total. In the pre-processing stage, the impactor was placed at the top centre of the laminate and away from the surface by 0.1 mm, as shown in Figure 1a. The movement of peripheral nodes of the laminate was fully constrained,

as shown in Figure 1b. The impactor was modelled by rigid body. Translation in the Z direction was the only degree of freedom allowed for the impactor, and the density of the impactor was corrected in order to match the mass of that used in the experiment. Figure 1c shows the mesh used where the shaded area is a structured mesh, and the unshaded areas are used for mesh transition. A fully contiguous mesh was used throughout the model, and nodes were merged between composite plies and interface layers. A Region-Of-Interest (ROI) of diameter 60 mm was defined at the centre of the plate. To accurately capture delamination propagation while considering the computational cost, the maximum element length in ROI was set less than 0.5 mm, which generates a total of 832,384 elements in the model. Segment-based contact was defined between impactor surface and top surface of the laminate model. Impact force was obtained from the penalty contact force generated by the contact pair. Solid elements (Type_1 in LS-Dyna) with eight nodes and one centrally located integration point were used for the plies, one element through the thickness of each ply block. 3D cohesive elements (Type_19 in LS-Dyna) were selected for use in the cohesive layers for modelling delamination. Type_19 is an 8 noded 4 integration point cohesive element, details of which can be found in [**Error! Reference source not found.**].

For explicitly accounting for matrix cracking in 'high-fidelity' modelling approaches, the numerical results [1436,44] show impact damage predictions were indeed improved by accounting for matrix cracking, but the level of improvement is limited. Here a more practical approach, suitable for some industrial applications, was adopted and used since models with individual cracks modelled have large computational requirements, and models without cracks are still suitable for comparative studies between materials, as presented here.

3.2 Material Properties and Formulations

Table 2 summarises the LS-Dyna material models used. The first is a standard model (Baseline), where fibre failure is predicted using MAT_261 [28,38,40], and delamination is predicted using MAT_138 [**Error! Reference source not found.**]. The second is a user defined material model (UMAT) where fibre failure and delamination are predicted using, respectively, UMAT_44 [**Error! Reference source not found.**] and UMAT_50 [**Error! Reference source not found.**]. These material models are concisely described below.

3.2.1 Translaminar failure models (Fibre Failure)

Two models (MAT_261 and UMAT_44) are implemented in this study where the MAT_261 model, [28,38,40], is based on Continuum Damage Mechanics (CDM) and can take into account damages associated with both matrix and fibre. As the overall stiffness degradation of a laminate due to matrix failure as the results of low-velocity impact is significantly smaller compared to that of delamination and fibre failure [**Error! Reference source not found.**], the

matrix failure modes were deactivated leaving only fibre failure modes being active. The damage propagation, beyond initial failure was defined by energy absorbed and corresponding fracture toughness

The UMAT_44 material model uses a Weibull statistically based tensile ($\sigma_{11} > 0$) fibre failure criterion [**Error! Reference source not found.**]. The survival probability (P_i) of a specimen with volume V under a stress of σ_i is represented by:

$$P_i(\sigma) = \exp\left(-\int_{V_i} \left(\frac{\sigma_i}{\sigma_0} \right)^m dV \right) \qquad \text{Equation 1}$$

where σ_0 and m are the characteristic strength and the Weibull modulus which is considered as a material property to describe the scatter of the strength in brittle and quasi-brittle materials. Using the assumption of equal probability of survival at the failure load level between fibres in a laminate and in a unit volume of material, we then have:

$$\exp\left(\sum_{i=1}^{N} -V_i \left(\frac{\sigma_i}{\sigma_{unit}} \right)^m \right) = 1 \qquad \text{Equation 2}$$

where N is the total number of elements. In scaled tensile tests, the σ_{unit} and m can be experimentally derived from plotting a least squares fit from a plot of σ against V *and* $\ln(\sigma)$ against $\ln(V)$, respectively [12]. When the probability of survival of a specimen satisfies:

$$\sum_{i=1}^{N} -V_i \left(\frac{\sigma_i}{\sigma_{unit}} \right)^m \geq 1 \qquad \text{Equation 3}$$

tensile failure occurs and the element with the highest stress is deleted. The Weibull criterion is evaluated again in the next time increment for progressive failure [**Error! Reference source not found.**]. For fibre compressive failure (when $\sigma_{11} < 0$), the failure criterion used is:

$$f_{fc} = -\frac{\sigma_{11}}{S_{fc}} = 1 \qquad \text{Equation 4}$$

where f_{fc} is an indicator for fibre compressive failure, σ_{11} and S_{fc} are the compressive stress and strength in fibre direction, respectively. The UMAT_44 model was applied in conjunction with element deletion option (elements are removed after failure via the standard LS-Dyna deletion procedure).

3.2.2 Interlaminar failure

The two LS-Dyna material models: MAT_138 [**Error! Reference source not found.**] and UMAT_50 [**Error! Reference source not found.**] used for delamination modelling are based on similar cohesive formulation. The UMAT_50 model was validated by experiments [**Error! Reference source not found.**]. Both models follow a bilinear traction displacement

law, with a strength based initiation criterion and an energy based propagation criterion. There are four input parameters required to characterise the constitutive law, namely initial penalty stiffness, *K*, strength (maximum tractions), $\sigma_I{}^{max}$ and $\sigma_{II}{}^{max}$, and the critical energy release rates in Mode I and II, i.e. G_{IC} and G_{IIC}, which follows Griffith's theory that fracture toughness is equal to the area under the traction-displacement jump relationship.

A unique feature of UMAT_50 is regarding the enhancement effect of compressive stress on shear properties, which increases the Mode II delamination initiation and propagation due to through-thickness compressive stress [48]. The Mode II traction and critical energy release rate are enhanced as:

$$\begin{cases} \sigma_{IIn}^{*} = \sigma_{II}^{*} - \eta\sigma_I \\ G_{IICn} = G_{IIC}^{*}\left(\frac{\sigma_{IIn}^{*}}{\sigma_{II}^{*}}\right) \end{cases} \quad when\ \sigma_I < 0 \qquad \text{Equation 5}$$

where σ_{IIn}^{*} and G_{IICn} are the enhanced Mode II strength and critical energy release rate and η is a material-dependent enhancement, see Table 1 for typical material properties used in the present work. It is noted that the enhancement factor used in this study is 0.3 which empirically derived from previous studies [**Error! Reference source not found.**]. The damage onset under mixed-mode loading is assumed to be controlled by a quadratic damage initiation law. In order to simulate damage growth under mixed-mode after damage onset, a fracture energy-based mixed-mode criterion B-K law was adopted, as shown below, see for instance [47]:

$$G_C = G_{IC} + (G_{IICn} - G_{IC})\left(\frac{G_{II}}{G_I + G_{II}}\right)^{\beta} \qquad \text{Equation 6}$$

where G_C and β is the mixed-mode energy release rate and B-K law exponent, respectively. In order to avoid element inversion during the impact loading, element deletion procedure was activated when MAT_138 model was implemented and hence additional contact was therefore defined between adjacent ply surfaces alongside each cohesive layer. The numerical models studied are summarised in Table 2 together with the impact cases. The models will be referred to as: Baseline, CDM and Discrete.

4. ANALYTICAL APPROACH

4.1 Critical threshold impact force

It is known that delamination propagation in composites tends to develop at a critical impact load and the theoretical critical force (P_{cr}) is given by [49]:

$$P_{cr} = \frac{\pi}{3}\sqrt{\frac{8\,E\,G_{IIC}}{1-\upsilon^2}}\,h^{3/2} \qquad \text{Equation 7}$$

where E is the effective Young's modulus of the laminate; h and υ are the thickness and Poisson ratio of the laminate. Readers are referred to reference [49] for more details of this analytical approach.

5. RESULTS

5.1 Comparison between experimental data

Figure 2 and Figure 3 show the results for the IM7/PEEK and IMS65/MTM materials tested under 8 J impact energy, and Figure 4 and Figure 5 are for the same materials tested under 30 J impact. Graphs are plotted for experimental and numerical results (by Baseline and CDM models) of force history, force-displacement curves, and delamination area.

Figure 6a and Figure 6b show comparisons between maximum energy absorbed, and Figure 6c shows the variation of the damage diameter with absorbed energy for both material and impact cases. Note that the straight lines drawn are not meant to imply a linear relationship between the energy and the predictions but are used to help the readers visualise the various trends of the various materials and models. The damage size was measured from the C-scan and the area of damage was converted into an equivalent damage diameter. Although the use of equivalent damage diameter masks any details about the shape of delaminated areas in the individual plies and the location of the highest area, it, nonetheless, gives a simple measure for comparison of the maximum size of the damage.

All the measured properties increased with increasing the impact energies but the rate of increase depended upon the property and the material tested. For instance, for the IMS65/MTM material, as the energy increases from 8 to 30 J (i.e. an increase in energy by 3.75 fold), the absorbed energy, maximum impact load, maximum deflection, damage diameter increased by factor of 3.49, 2.27, 1.93 and 2.15, respectively. A similar trend was observed in the case of IM7/PEEK material.

For IMS65/MTM laminates under both 8 J and 30J impact the measured force histories (Figure 3a and Figure 5a) and damage sizes (Figure 3c and Figure 5c), were found to be more consistent, compared to IM7/PEEK laminates, as shown in Figure 2a and Figure 4a. An experimental scatter in the IM7/PEEK results was found in load history and damage size, for both energy cases. The measured damage size was related to the first significant load drop in the force time history and amount of energy absorbed. For instance, at 8 J impact energy, the damage size varied from 6mm to 24mm, and at 30 J the diameter ranges from 48 mm to 63 mm.

5.2 Impact Force

The critical force causing delamination P_{cr} for IM7/PEEK can be calculated from Eq.7, to be ~7.4 kN. The maximum measured forces in the 8 J impact are close to the theoretical threshold value, therefore it is possible that in some of the tests there will be no unstable delamination propagation. As the delamination is too small to affect the global stiffness of the plate, the force history of this case exhibits a nearly perfect half sines wave shape. In the rest of the cases, delaminations are large enough to degrade the stiffness of the plate and cause vibration when the plate suddenly changes its state, giving a significant load drop in each curve, as shown in Figure 2a.

The scatter in the delamination area measured in IM7/PEEK under 8 J impact may be attributed to an existence of an energy threshold for rapid growth of delamination. In order to verify this hypothesis, simulations were conducted under the impact energies below and above 8 J to try to understand the relation between impact energies and delaminations. The two energy levels chosen were 6 J and 10 J. These verification models used the CDM modelling approach. The results showed that the delamination diameters increase linearly with increasing impact energies giving 5.4 mm, 7.4 mm and 9.4 mm delamination diameter from 6 J, 8 J and 10 J impact models, respectively. These additional modelling results are very much in line with the trend of experiment results in [**Error! Reference source not found.**]. The delamination diameter of the IM7/PEEK 8 J case is ~23 mm and significantly larger than the predicted 10 J case. Experimental observations, verification models and those studies in [**Error! Reference source not found.**] may indicate that the linear relation between delamination area and impact energy may be attributed to material behaviour of IM7/PEEK not being captured in the models using the material properties provided in Table 1.

A comparison between the experimental and simulation results of force-histories for the IMS65/MTM laminate at 8 J impact is made in Figure 3. The predicted maximum load from baseline model is slightly higher than that predicted from the CDM model. Both predictions were greater than that measured from the tests and do not show any significant load drops on the curves. The load (P_{cr}) of the IMS65/MTM was calculated to be ~ 5.3 kN which is close to the experimental results, as shown in Figure 3. It can be seen from Eq.7 that the critical force is proportional to $\sqrt{G_{IIC}}$. Neglecting the minor differences in ply properties between the two materials (see Table 1), the critical load (P_{cr}) for the IM7/PEEK can be expected to be higher than that for the IMS65/MTM, by a factor of ~1.4. Comparing the experimental critical loads of both laminates, the ratio is ~1.2 (= 6.7/5.5) and lower than the theoretical ratio. Although the critical load in the form a significant load drop in force history is not captured in the numerical model, the load level when delamination starts to propagate can be extracted from post-

processing of the FEA simulations. Figure 7 shows a normalised (simulation results were divided by mean experimental critical load) critical load of all models under 30 J impact.

Figure 8 shows a comparison between the predicted and measured maximum force for all cases. In general, except for the IMS65/MTM at 8 J case, all predicted maximum forces are within an acceptable range. The experimental data indicated that the IM7/PEEK exhibited larger maximum force than the IMS65/MTM material. Most of the models captured the same trend. The analytical critical loads predicted from Eq(6) are 7.4 kN and 5.3 kN for the IM7 and the IMS65 materials, respectively. These analytical values are slightly higher than the predictions of the FE models. Table 4 gives a summary of the predicted results for both materials and both impact energies.

It should be noted here that none of the models used here considered matrix cracking and their potential effects on creating more delamination and on absorbing some of the impact energy. The role played by matrix cracks and their influence on the impact response of composites was discussed in Abisset et al [**Error! Reference source not found.**]. The predicted delamination load, using the Eq.7, was some 20% higher than the measured loads. They attributed that to the presence of transverse cracks prior to delamination where these cracks help the occurrence of delamination by creating stress concentration at the interfaces.

5.3 Delamination

Given that the interfacial properties of IMS65/MTM are significantly lower than the IM7/PEEK, the delamination damage in IMS65/MTM can be expected to initiate at a lower force level. In fact its damage sizes are only slightly smaller than the IM7/PEEK laminate (see Figure 6c). These observations imply that the G_{IIC} used for the IM7/PEEK material, as shown in Table 1, taken from the literature [**Error! Reference source not found.**], in which the fracture toughness was measured under static condition may not be suitable for these impact simulations. Therefore, additional simulations were performed using a lower G_{IIC} value to directly correlate the experimental observations. The G_{IIC} value of 1.5 N/mm instead of 2.2 N/mm was selected and compared with original simulation, and the force history results with corresponding delamination predictions are shown in Figure 9. It can be seen that the use lower G_{IIC} value for the CDM models gives better correlation with experimental results compared to that given in Table 1. Similar observations and approach were also reported and adopted in [3262], in which impact damage prediction of IM7/PEEK laminate was significantly improved when G_{IIC} was reduced from 2 N/mm to 0.4 N/mm for 20 J impact. They measured G_{IIC}, using ENF method, for carbon/PEEK materials and showed that the values ranged from 1.9 N/mm, for stable (ductile) crack growth at low strain rate, to 0.4 N/mm, corresponding to unstable crack propagation at high strain rate [**Error! Reference source not found.**].

In addition, the projected delamination shape of the IMS65/MTM laminate appears to be somewhat irregular, and the delamination shapes of the IM7/PEEK cases are closer to circular and appear to be less repeatable than the IMS65/MTM laminates. These repeatable delaminations with irregular shapes for the two given impact energies in the IMS65/MTM laminate are shown in Figure 5c. The highly directional behaviour, especially at 30 J (Figure 5c), may be attributed to the existence of strong interaction between delamination and matrix cracks.

Similar observations regarding the shape of damage areas of thermoset and thermoplastic carbon composites laminates were observed by Nezhad et al [**Error! Reference source not found.**]. They attributed that to bending matrix cracks at the bottom most [0^o] ply and the larger strain to failure beyond the yielding of the PEEK. Another study showed that the fracture surface of the PEEK composite for pure mode I to pure mode II have cusps caused by the higher amount of matrix plasticity. In contrast, in epoxy composites the fracture surfaces of lower modes are completely flat indicating brittle cleavage fracture. Hackles appear with higher mode-mixity in an epoxy composite, whereas no hackle formation is observed in PEEK [**Error! Reference source not found.**].

The equivalent damage diameter is underestimated by the baseline models for the IMS65/MTM in the 8J case but is overestimated, by a factor of up to 2, in 30 J case. It is worth mentioning that this large overshoot of the prediction in this case came from over predicted delaminations at interfaces near mid-plane of the laminate where delamination propagated to the boundary of the plate. As the mesh size becomes coarse (see Figure 1), the prediction tends to be less accurate for the baseline model.

The use of reliable input data is crucial for the all the models. Given that the predicted delamination areas are overestimated in both models under 30 J impact for the IMS65/MTM, the current interfacial properties of the IMS65/MTM material, taken from [**Error! Reference source not found.**], may be slightly different to those of the panels, and the formulation governing the propagation of the delamination could be affected. However, data available on IMS65/MTM are quite sparse.

5.4 Comparison between Numerical Models

5.4.1 Baseline and CDM Models

All models gave good predictions for maximum impact force and maximum deflection for both materials in both 8 J and 30 J impact cases (see from Figure 2 to Figure 5). Difference between the baseline and CDM model came from the application of cohesive formulations MAT_138 and UMAT_50. However, the impact energy absorbed and damage areas were generally under-predicted and the degree of correlation depended upon the types of modelling

approach (see Figure 6). In general, the CDM models gave better predictions for energy absorption in most of the cases compared to the baseline models, but the predictions are all lower than the experimental results, except for the IMS65/MTM at 30 J case.

The numerical results from the baseline and CDM models, regardless of their accuracy, gave highly consistent results that can be fully explained by the theories and formulations used in the study. Due to lower interfacial properties, the delamination areas in the IMS65/MTM under both 8 J and 30 J impacts are higher than those in the IM7/PEEK.

The numerical models predicted the delamination to be spread throughout the thickness of the laminates. Figure 11 shows an example of the results of the distribution of delamination size from the CDM and Baseline FE models for 8 and 30 J impact, where the impacted surface is that at the top. A study of delaminations through the thickness shows the following features:

- The number of delaminated surfaces depends on the type of materials, impact energy and the type of models used. For the 30 J impact, and for IMS65/MTM material, the number of delaminated surfaces are 19 and 22 using, respectively, CDM (UMAT) and Baseline models. For the IM7/PEEK materials, the numbers are 14 and 19 for the CDM and Baseline models, respectively.

- Generally, especially for the high impact energy, delaminated sizes are not uniform through the thickness, with the maximum area (largest diameter) occurring close to the middle section of the panels. For the IMS65/MTM materials, the maximum delamination took place at interfaces 13 and 14 whereas for the IM7/PEEK materials, the maximum is at interface 11.

- The number of delaminated area increases with increasing the impact energy.

- As a result of using an enhancement of the critical energy release rate, Eq.5, the delamination was reduced (suppressed) near in the impacted surfaces for the IM7/PEEK (Interfaces 24-21 at 30J impact and Interfaces 24-16 at 8 J impact). Experimental results are not available at the present to validate this behaviour.

5.4.2 Comparison between CDM and Discrete Models at 30 J

Figure 5a shows experimental and numerical force-displacement curves for the IMS65/MTM laminate under 30 J impact. The correlation between measured and predicted curves is reasonable in terms of the maximum displacements and maximum loads. It can be seen that the overall plate stiffness of the discrete model (Figure 5b) has the highest stiffness among other models. Although, delamination propagation was not traceable from the force history curves in numerical models, the predicted critical loads could be extracted from the corresponding impact force as delamination starts to grow in the simulation. A critical force in

IMS65/MTM in the discrete model at 30 J case corresponds to a plateau of the force-displacement curve; a clear stiffness decrease can be seen after the critical load has been reached, as shown in Figure 5b. This clear stiffness change found in the discrete model is not observed in the baseline and CDM model.

Figure 10 compares the force history for 30 J impact using CDM and discrete modelling approaches for the IMS65/MTM. In general, the impact responses between the two approaches within one material system are similar, and their differences are fairly consistent across the two laminates. It seems there are more force oscillations in the discrete model, which may be due to the brittle-like failure behaviour of plies in UMAT_44. As the fibre damage propagation is controlled by a continuous bi-linear law in the CDM models, the force oscillations appear to be less. The global plate stiffness from the beginning of impact is consistently lower in the CDM model than in the discrete model for both laminates. This behaviour may be related to the compressive damage evolution applied in the CDM approach affecting the compressive failure behaviour under the impactor. As the impactor rebounds, Figure 4b and Figure 5b show a positive final displacement in the CDM model for both laminates, which indicates irreversibly damaged elements in compression. This positive displacement, representing permanent damage, is an agreement with test data.

In Figure 10 it can be seen that a load drop in the CDM model leads to a stiffness reduction in the force-displacement curve when the impact force reaches 12 kN. This load drop may indicate the commencing of stiffness degradation scheme in CDM approach. In contrast, the force in the discrete models continues to increase without any significant load drop. Due to the fracture energy based damage propagation criterion in CDM model, energy absorbed in both laminates are higher than that using discrete method.

5.4.3 Fibre Damage

Fibre failure was predicted by the FE models developed in the present work. Fibre failure is a crucial failure mode and the energy required to cause such a mode of failure is much larger than that for delamination and for matrix cracking. Figure 10 shows the development of fibre direction stress of the bottom most (0^o) ply at different stages in IMS65/MTM 30 J impact models in the discrete and CDM approaches. It can be seen that the stress field of the discrete model is localised and tensile failure occurs much earlier than that in the CDM model. The failed and deleted elements in the discrete model consist of a narrow 'failure band' which is similar to a realistic fibre breakage, and the crack propagates as stresses at crack tips exceed the strength level.

In the CDM model, due to the inclusion of compressive failure formulation, the deflection of the plate is less localised due to the deformation of compressively damaged

elements, and the stress field in elements subjected to tension is more smeared, and the damaged elements are still under moderate stress before complete failure. For all the CDM models, once the tensile failure onset criterion is reached and the stiffness of the damaged elements starts to degrade, the stress concentration tends to migrate to adjacent healthy elements and even to neighbouring plies; as a result, it is difficult to generate a band of completely failed elements as shown in the discrete model. These numerical results suggest that the CDM models may provide reasonable end results, but detailed failure behaviour such as the tensile failure in the bottom most plies during impact of the laminate is not captured as realistically as the discrete model using simple stress-based criterion.

5.5 Further Discussion

Reasons for the experimental scatter and disagreements between test and modelling for the IM7/PEEK results are not fully understood but the following qualitative arguments are relevant in providing plausible explanations.

5.5.1 Elastic perfectly plastic behaviour

The PEEK material, as a pure resin, behaves in ductile manner with stress strain curves akin to elastic perfectly plastic material [**Error! Reference source not found.**]. After reaching the yield stress, the stress exhibits a constant plateau with increasing strain, which implies that the material will deform extensively while the load (stress) remains virtually constant. This behaviour could give a rise to unstable damage/delamination behaviour. The current models do not take into account this aspect of failure of the PEEK material.

5.5.2 Effects of crystallinity

The effect of degree of crystallinity was initially thought to be a major factor causing differences. It is known [56,58] that the degree of crystallinity in PEEK plays a major role in the response of PEEK-based materials to mechanical loading. Measurements have been made in the present work of the degree of crystallinity of the PEEK materials tested here using thermal analysis methods (DSC) [**Error! Reference source not found.**]. The results showed that there was no clear correlation between the degree of crystallinity and impact data in this study.

5.5.3 Uncontrolled delamination propagation

Some of the previous work on PEEK composites had shown that damage can be developed in an uncontrolled fashion. Experimental work reported in [**Error! Reference source not found.**] on 2.5 mm thick laminates made of $(\pm 45/0_3/\pm 45/0_2)_s$ lay-up showed that the damage area for PEEK material varies considerably between tests for the same impact energy, when compared with carbon/epoxy laminates. For an impact energy of 7 J, the damage area in the PEEK laminates ranged from around 2 cm^2 to 6 cm^2 whereas that for the epoxy laminate

was consistently around 6.2 cm^2. Modes of failure played a major role in the damage area creation. Unstable delamination propagation in PEEK materials has been observed by Brunner et al [**Error! Reference source not found.**]. Nezhad et al [**Error! Reference source not found.**] presented experimental results showing that for the same lay-up and the thickness, impact energy, the damage areas exhibited in the PEEK carbon laminates were larger than those of epoxy carbon laminates.

5.5.4 Testing methods for fracture toughness

Values of G_{Ic} and G_{IIc} are normally obtained from testing 0° unidirectional samples. Hiley [**Error! Reference source not found.**] discussed the phenomenon of the 'R-curve effect' for mode I dominated loading where the toughness increases with crack length which introduces problems when generating structural data. This effect is attributed to fibre bridging which is an artefact of testing 0° laminates and will not occur in practice where delaminations occur at non-zero ply interfaces, in which nesting and consequently fibre bridging is negligible. Tests conducted on 0°/5° ply interfaces have been used to eliminate fibre bridging but to still characterise the toughness of unidirectional ply interfaces. Also, in real structures, delaminations appear between plies of different orientation, while most tests are done on unidirectional specimens. Ideally, delamination testing should be carried out on multidirectional laminates, which have a thicker resin rich zone.

Early work [63] on measuring G_{IIc} for thermoset and thermoplastic composites using ENF technique showed that, while epoxy-based composites exhibited a small scatter (less than 10%)) the AS4/PEEK composites showed a wide scatter, reaching 20%. The 20% scatter was more obvious in the G_{IIc} corresponding to the start of nonlinearity in the load-displacement curve. Brittle and toughened epoxies fail by hackle formation but very tough matrix systems (PEEK) fail by extensive shear yielding. Tanaka et al [**Error! Reference source not found.**] reported a scatter in the start of nonlinearity of the curves of around 45%. Currently, there is no consensus on test methods and available test data show a large scatter. Common test geometries show unstable delamination growth.

5.5.5 Visco-elastic and plastic and dynamic effects

The visco-elastic and visco-plastic behaviour of PEEK materials is widely recognised [65], and consequently, one of the key differences between the behaviour of epoxy-based and PEEK-based composites is that strain rate effects could be influential. A study made in [**Error! Reference source not found.**] has shown that static and dynamically loaded PEEK and epoxy based samples exhibited comparable energy absorptions. However, the impacted laminates, especially the PEEK-based, showed larger extensions of delaminations and, at the same time, smaller amounts of fibre fracture. The variation in the dominant damage modes with impact

velocity implies a clear rate-sensitivity of the material, a probable consequence of the viscoelastic nature of the PEEK matrix. Recent work by Sun [**Error! Reference source not found.**] has also indicated the importance of strain rate on the impact response.

6. CONCLUSIONS

A comparative study has been carried out on thermoset and thermoplastic based carbon fibre composites panels where their behaviour was studied experimentally and numerically under low impact velocity, at two key impact energies (8 J and 30 J). A Standard (baseline) model and two improved material (continuum damage mechanics (CDM) and discrete) models using LS-DYNA code were implemented. The models were designed to provide medium-fidelity prediction with reasonable computational cost.

The three numerical models gave generally reliable predictions of the measured maximum impact force and the maximum central deflection of the panels. The baseline model was shown to give less favourable correlation with test data than the CDM model when predicting the damage (delamination) area and the energy absorbed. The discrete model also underestimated the measured maximum impact force, due to its fibre failure assumption and gave lower predictions than those of the CDM model, at 30J.

The experimental data on thermoplastic panels seem to exhibit large variation in the damage development and unstable damage growth compared with the thermoset panels.

The use of manufacturer's data on fracture toughness for Mode II (2.2 N/mm) of the thermoplastic materials leads to an underestimation of the energy absorbed and damage size. Similar observation was recently made in [**Error! Reference source not found.**]. There is a need to understand the susceptibility of this material to uncontrolled damage development and strain rate effects [**Error! Reference source not found.**]. Nonetheless, there was a clear trend between the energy absorbed and delamination size at a given impact energy.

Experimental results showed the projected delamination areas observed in the thermoset material are highly directional, which indicates strong interaction between matrix cracks and delaminations and suggests that modelling of the matrix cracks may be required for high-fidelity numerical predictions [**Error! Reference source not found.**].

Detailed microscopic experimental data describing the amount and the location of the different damage modes are unavailable and future work is required for a deeper understanding of this aspect.

7. ACKNOWLEDGEMENTS

The work was a part of a MAST project sponsored by DSTL on behalf of the UK Ministry of Defence. The authors would like to thank sponsors for their support. The authors would also like to thank Peter Hopgood (DSTL) and Kevin Denham (DSTL) for their technical leadership.

8. REFERENCES

1. Chou I, Inutake T, Namba K. Correlation of damage resistance under low velocity impact and Mode II delamination resistance in CFRP laminates. Advanced Composite Materials 1999;8:167-76. doi:10.1163/156855199X00173.

2. Dorey G, Bishop SM, Curtis PT. On the impact performance of carbon fibre laminates with epoxy and PEEK matrices. Composites Science and Technology 1985;23:221-37. doi:10.1016/0266-3538(85)90019-3.

3. Bishop S, M. The Mechanical performance and impact behaviour of carbon-fibre reinforced PEEK. Composite Structures 1985;3 pp 295 318.

4. Roux M, Eguémann N, Dransfeld C, Thiébaud F, Perreux D. Thermoplastic carbon fibre-reinforced polymer recycling with electrodynamical fragmentation. Journal of Thermoplastic Composite Materials 2017;30:381-403. doi:10.1177/0892705715599431.

5. Schuck M. New processes for mass production of thermoplastic composite lightweight components. European Conference On Composite Materials 2012:24-8.

6. Morita H, Adachi T, Tateishi Y, Matsumot H. Characterization of impact damage resistance of CF/PEEK and CF/toughened epoxy laminates under low and high velocity impact tests. Journal of Reinforced Plastics and Composites 1997;16:131-43. doi:10.1177/073168449701600203.

7. Ishikawa T, Sugimoto S, Matsushima M, Hayashi Y. Some experimental findings in compression-after-impact (CAI) tests of CF/PEEK (APC-2) and conventional CF/epoxy flat plates. Composites Science and Technology 1995;55:349-63. doi:10.1016/0266-3538(95)00079-8.

8. Maio L, Monaco E, Ricci F, Lecce L. Simulation of low velocity impact on composite laminates with progressive failure analysis. Composite Structures 2013;103:75-85. doi:10.1016/j.compstruct.2013.02.027.

9. Feng D, Aymerich F. Finite element modelling of damage induced by low-velocity impact on composite laminates. Composite Structures 2014;108:161-71. doi:10.1016/j.compstruct.2013.09.004.

10. Shi Y, Pinna C, Soutis C. Modelling impact damage in composite laminates: A simulation of intra- and inter-laminar cracking. Composite Structures 2014;114:10-9. doi:10.1016/j.compstruct.2014.03.052.

11. González EV, Maimí P, Camanho PP, Turon A, Mayugo J. Simulation of drop-weight impact and compression after impact tests on composite laminates. Composite Structures 2012;94:3364-78. doi:10.1016/j.compstruct.2012.05.015.

12. Lopes CS, Sádaba S, González C, LLorca J, Camanho PP. Physically-sound simulation of low-velocity impact on fiber reinforced laminates. International Journal of Impact Engineering 2015:1-15. doi:10.1016/j.ijimpeng.2015.05.014.

13. Batra RC, Gopinath G, Zheng JQ. Damage and failure in low energy impact of fiber-reinforced polymeric composite laminates. Composite Structures 2012;94:540-7. doi:10.1016/j.compstruct.2011.08.015.

14. Sun XC, Wisnom MR, Hallett SR. Interaction of inter- and intralaminar damage in scaled quasi-static indentation tests: Part 2 - Numerical simulation. Composite Structures 2016;136. doi:10.1016/j.compstruct.2015.09.062.

15. Sun XC, Hallett SR. Barely visible impact damage in scaled composite laminates: Experiments and numerical simulations. International Journal of Impact Engineering 2017;109. doi:10.1016/j.ijimpeng.2017.06.008.

16. Faggiani A, Falzon BG. Predicting low-velocity impact damage on a stiffened composite panel. Composites Part A: Applied Science and Manufacturing 2010;41:737-49. doi:10.1016/j.compositesa.2010.02.005.

17. Donadon MV, Iannucci L, Falzon BG, Hodgkinson JM, de Almeida SFM. A progressive failure model for composite laminates subjected to low velocity impact damage. Computers & Structures 2008;86:1232-52. doi:10.1016/j.compstruc.2007.11.004.

18. Raimondo L, Iannucci L, Robinson P, Curtis PT. A progressive failure model for mesh-size-independent FE analysis of composite laminates subject to low-velocity impact damage. Composites Science and Technology 2012;72:624-32. doi:10.1016/j.compscitech.2012.01.007.

19. Tan W, Falzon BG, Chiu LNS, Price M. Predicting low velocity impact damage and Compression-After-Impact (CAI) behaviour of composite laminates. Composites Part A: Applied Science and Manufacturing 2015;71:212-26. doi:10.1016/j.compositesa.2015.01.025.

20. González EV. Simulation of interlaminar and intralaminar damage in polymer-based composites for aeronautical applications under impact loading. Ph.D. thesis. Universitat de Girona; 2010.

21. Lopes CS, Camanho PP, Gürdal Z, Maimí P, González EV. Low-velocity impact damage on dispersed stacking sequence laminates. Part II: Numerical simulations. Composites Science and Technology 2009;69:937-47. doi:10.1016/j.compscitech.2009.02.015.

22. González EV, Maimí P, Camanho PP, Lopes CS, Blanco N. Effects of ply clustering in laminated composite plates under low-velocity impact loading. Composites Science and Technology 2011;71:805-17. doi:10.1016/j.compscitech.2010.12.018.

23. Shi Y, Swait T, Soutis C. Modelling damage evolution in composite laminates subjected to low velocity impact. Composite Structures 2012;94:2902-13. doi:10.1016/j.compstruct.2012.03.039.

24. Hallett SR, Wisnom MR. Numerical investigation of progressive damage and the effect of layup in notched tensile tests. Journal of Composite Materials 2005;40:1229-45. doi:10.1177/0021998305057432.

25. Hallett SR, Green BG, Jiang WG, Wisnom MR. An experimental and numerical investigation into the damage mechanisms in notched composites. Composites Part A: Applied Science and Manufacturing 2009;40:613-24. doi:10.1016/j.compositesa.2009.02.021.

26. Hou JP, Petrinic N, Ruiz C, Hallett SR. Prediction of impact damage in composite plates. Composites Science and Technology 2000;60:273-81. doi:10.1016/S0266-3538(99)00126-8.

27. Hallett SR, Green BG, Jiang W-G, Cheung KH, Wisnom MR. The open hole tensile test: a challenge for virtual testing of composites. International Journal of Fracture 2009;158:169-81. doi:10.1007/s10704-009-9333-8.

28. Pinho ST, Iannucci L, Robinson P. Physically-based failure models and criteria for laminated fibre-reinforced composites with emphasis on fibre kinking: Part I: Development. Composites Part A: Applied Science and Manufacturing 2006;37:63-73. doi:10.1016/j.compositesa.2005.04.016.

29. Jiang W, Hallett S, Wisnom M. Modelling of damage in composite materials using interface elements. 5th European LS-Dyna Users Conference 2005.

30. Tsampas S. Analysis of compression failure in multidirectional laminates. South Kensington campus Imperial college London, 2013. PhD thesis.

31. Cytec Engineered Materials. Technical data sheet of APC-2-PEEK Thermoplastic Polymer, AECM-000 0 40, March 2012, www.cytec.com

32. Bouvet C, Dau F, Peres P, Defence A. Low Velocity impact on laminate composite with thermoplastic resin. DYNCOMP 2015 2015:2-5.

33. Reeder JR. 3-D Mixed mode delamination fracture criteria - an experimentalist's perspective. Proceedings Of Annual Technical Conference Of The American Society For Composites 2006;21:17-20.

34. Naghipour P, Bartsch M, Voggenreiter H. Simulation and experimental validation of mixed mode delamination in multidirectional CF/PEEK laminates under fatigue loading. International Journal of Solids and Structures 2011;48:1070-81. doi:10.1016/j.ijsolstr.2010.12.012.

35. Department CUE. Materials Data Book 2003.

36. Abisset E, Daghia F, Sun XC, Wisnom MR, Hallett SR. Interaction of inter- and intralaminar damage in scaled quasi-static indentation tests: Part 1 - Experiments. Composite Structures 2016;136:712-26. doi:10.1016/j.compstruct.2015.09.061.

37. Elmarakbi a. M, Hu N, Fukunaga H. Finite element simulation of delamination growth in composite materials using LS-DYNA. Composites Science and Technology 2009;69:2383-91. doi:10.1016/j.compscitech.2009.01.036.

38. Livermore Software Technology Corporation (LSTC). LS-DYNA keyword User's Manual Volume II Material Models. LS-DYNA R80 2015.

39. Li X, Hallett SR, Wisnom MR. A finite element based statistical model for progressive tensile fibre failure in composite laminates. Composites Part B: Engineering 2013;45:433-9. doi:10.1016/j.compositesb.2012.08.001.

40. Pinho ST, Iannucci L, Robinson P. Physically based failure models and criteria for laminated fibre-reinforced composites with emphasis on fibre kinking. Part II: FE implementation. Composites Part A: Applied Science and Manufacturing 2006;37:766-77. doi:10.1016/j.compositesa.2005.06.008.

41. Sun XC. Impact Modelling of Composites. University of Bristol, UK, 2016.

42. Wisnom MR, Khan B, Hallett SR. Size effects in unnotched tensile strength of unidirectional and quasi-isotropic carbon/epoxy composites. Composite Structures 2008;84:21-8. doi:10.1016/j.compstruct.2007.06.002.

43. Jiang W-G, Hallett SR, Green BG, Wisnom MR. A concise interface constitutive law for analysis of delamination and splitting in composite materials and its application to scaled

notched tensile specimens. International Journal for Numerical Methods in Engineering 2007;69:1982-95. doi:10.1002/nme.1842.

44. Hallett SR, Jiang W-G, Khan B, Wisnom MR. Modelling the interaction between matrix cracks and delamination damage in scaled quasi-isotropic specimens. Composites Science and Technology 2008;68:80-9. doi:10.1016/j.compscitech.2007.05.038.

45. Gan KW, Wisnom MR, & Hallett SR. Effect of high through thickness compressive stress on fibre direction tensile strength of carbon/epoxy composite laminates. Composites Science and Technology, 90, 1-8. DOI: 10.1016/j.compscitech.2013.10.010, 2014.

46. Belnoue J P-H, Giannis S, Dawson M, Hallett, SR. Cohesive/adhesive failure interaction in ductile adhesive joints Part II: Quasi-static and fatigue analysis of double lap-joint specimens subjected to through-thickness compressive loading', International Journal of Adhesion and Adhesives, 2016; 68: 369-378. Doi:10.1016/j.ijadhadh.2016.03.010.

47. Camanho P, Davila CG. Mixed mode decohesion finite elements for the simulation of delamination in composite materials, NASA/ TM-2002- 211737, 2002.

48. Li X, Hallett SR, Wisnom MR. Predicting the effect of through-thickness compressive stress on delamination using interface elements. Composites Part A: Applied Science and Manufacturing 2008;39:218-30. doi:10.1016/j.compositesa.2007.11.005.

49. Davies GAO, Robinson P, Robson J, Eady D. Shear driven delamination propagation in two dimensions. Composites Part A: Applied Science and Manufacturing 1997;28:757-65. doi:10.1016/S1359-835X(97)00015-8.

50. Berger L, Cantwell W. Temperature and loading rate effects in the mode II interlaminar fracture behavior of carbon fiber reinforced PEEK. Polymer Composites 2001:271-81.

51. Kaddour AS and Lord SJ. Literature review & numerical modelling of composite panels under impact. QINETIQ/MS/AD/PUB1505304/1.0, Dec 2015.

52. Escale L, De Almeida O, Bernhart G and Ferrero J F. Comparison of the impact resistance of carbon/epoxy and carbon/peek composite laminates. Presented at 15th European Conference on Composite Materials: Composites at Venice, ECCM 2012; Venice; Italy; 24-28 June 2012.

53. Brunner AJ, Murphy N, Pinter G, Development of a standardized procedure for the characterization of interlaminar delamination propagation in advanced composites under fatigue mode I loading conditions. Engineering Fracture Mechanics; 76(18): 2678-2689, 2009.

54. Nezhad HY, Auffray A, McCarthy CT and O'Higgins R. Impact damage response of carbon fibre-reinforced aerospace composite panels. 20th International Conference on Composite Materials, Copenhagen, 19-24th July 2015

55. Rae P J, Brown EN and Orler EB. The mechanical properties of poly(ether-ether-ketone) (PEEK) with emphasis on the large compressive strain response. Polymer, V48, pp 598-615, 2007.

56. Talbott MF, Springer GS, Berglund LA. The effects of crystallinity on the mechanical properties of PEEK polymer and graphite fiber reinforced PEEK. J Compos Mater,; V21: 1056-81,1987

57. Alberola ND, Mele P, Bas C. Tensile mechanical properties of PEEK films over a wide range of strain rates II. J Appl Polym Sci; V64:1053-9, 1997.

58. Dahoun A, Aboulfaraj M, G'Sell C, Molinari A, Canova GR. Plastic behavior and deformation textures of poly(ether ether ketone) under uniaxial tension and shear. Polym Eng Sci; V35:317-30, 1995.

59. Chen F, Ou H, Gatea S, Long H. Hot tensile fracture characteristics and constitutive modelling of polyether-ether-ketone (PEEK). Polymer Testing, V 63, pp 168-179, 2017.

60. Aymerich F, Priolo P and Vacca D. Static loading and low-velocity impact characterization of graphite/PEEK laminates. NDT.net - March 1999, Vol. 4 No. 3.

61. Hiley MJ. Fractographic aspects of fatigue failure in composite materials. QINETIQ/FST/SMC/TR012369.

62. Bouvet C, Cheetah, A, Lisle, T, Ballere, L and Peres, P. Measure of rate sensitivity of mode ii interlaminar fracture toughness using infrared thermography. in 5th ECCOMAS, Composites2105, Bristol, UK, 2015.

63. Hiley MJ and Curtis PT. Mode II damage development in carbon fibre reinforced plastics. AGARD conference proceedings 530, 74th Meeting of the AGARD Structures and Materials Panel, held in Patras, Greece, May 1992.

64. Tanaka K, Kageyama K and Hojo K. Prestandardization study on mode II interlaminar fracture toughness test for CFRP in Japan. Composites, V26, pp 257 267, 1995.

65. Garcia-Gonzalez D, Rusinek A, Jankowiak T, Arias A. Mechanical impact behavior of polyether-ether-ketone (PEEK). Composite Structures, V 124, pp 88-99, 2015.

9. TABLES AND FIGURES

Table 1: Mechanical properties of IM7/PEEK and ISM65/MTM [30-**Error! Reference source not found.**]. It is noted that the fracture toughness value are quoted in N/mm for consistency with cohesive element formulation (1 N/mm = 1000 J/m^2)

Lamina properties	IM7/PEEK	IMS65/MTM
Density (Kg/m^3)	1596	1552
Longitudinal modulus E_1 (GPa)	170	175.9
Transverse modulus E_2 (GPa)	10	8.1
In-plane shear modulus G_{12} (GPa)	5.5	4.4
Minor Poisson's ratio	0.0158	0.0147
Through-thickness shear modulus G_{23} (GPa)	3.355	2.718
Through-thickness Poisson's ratio u_{32}	0.49	0.49
Longitudinal tensile strength X_T (MPa)	2900	3289
Longitudinal compressive strength X_C (MPa)	1310	1595
Transverse tensile strength Y_T (MPa)	60	56
Transverse compressive strength Y_C (MPa)	250	193
Fracture toughness for longitudinal (fibre) tensile failure (kJ/m^2)	100	90
Fracture toughness for longitudinal (fibre) compressive failure (kJ/m^2)	80	80
Weibull modulus (m)	41	41
Interface properties	**IM7/PEEK**	**IMS65/MTM**
Density (kg/cm^3)	1320	1180
Modulus (GPa)	100	100
Transverse and normal failure stress (MPa)	80	60
Interlaminar shear failure stress (MPa)	100	80

Interface fracture toughness for opening mode (N/mm)	1.6	0.38
Interface fracture toughness for shear mode (N/mm)	2.2	1.14
*B-K exponential β**	2.3	2.3
*Enhancement factor η***	0.3	0.3

(*) used in Eq.6 in this paper (**) used in Eq.5 in this paper

Table 2: Material models used for impact simulations.

Damage modes	*Material models*	
	LS-Dyna standard	*LS-Dyna user-defined(UMAT)*
Fibre failure	MAT_261 (CDM)	UMAT_44 (Discrete)
Delamination	MAT_138 (Cohesive formulation)	UMAT_50 (Advanced cohesive formulation)

Table 3: Cases of numerical modelling with the corresponding material models used and their element deletion scheme.

	Material models	IM7/PEEK		IMS65/MTM	
		8J	30J	8J	30J
Baseline($)	MAT_261/MAT_138	X			
CDM	MAT_261/UMAT_50	X(*)		X	X
Discrete	UMAT_44/UMAT_50	---	X	---	

($) Element deletion Enabled.
(X) Models using input data in Table 1.
(*) Models using input data in Table 1 in addition to other reduced values for G_{IIC}.
(---) No model used

Table 4: A summary of the predicted results for the maximum contact force, maximum displacement and energy absorbed for all cases performed for both lay-ups.

Model type	Energy absorbed (J)		Max force (N)		Max displacement (mm)	
	Material		Material		Material	
	IMS/MTM	IM7/PEEK	IMS/MTM	IM7/PEEK	IMS/MTM	IM7/PEEK
	At impact energy = 8 J					
CDM	3.27	3.16	6511	6843	2.01	1.81
Baseline	3.80	3.306	5921	6397	2.07	1.94
At impact energy = 30 J						
CDM	18.03	14.02	11742	13534	4.45	4.17
Baseline	17.69	13.50	12771	14081	4.56	3.87
Discrete	11.22	10.76	14148	13672	4.13	3.88

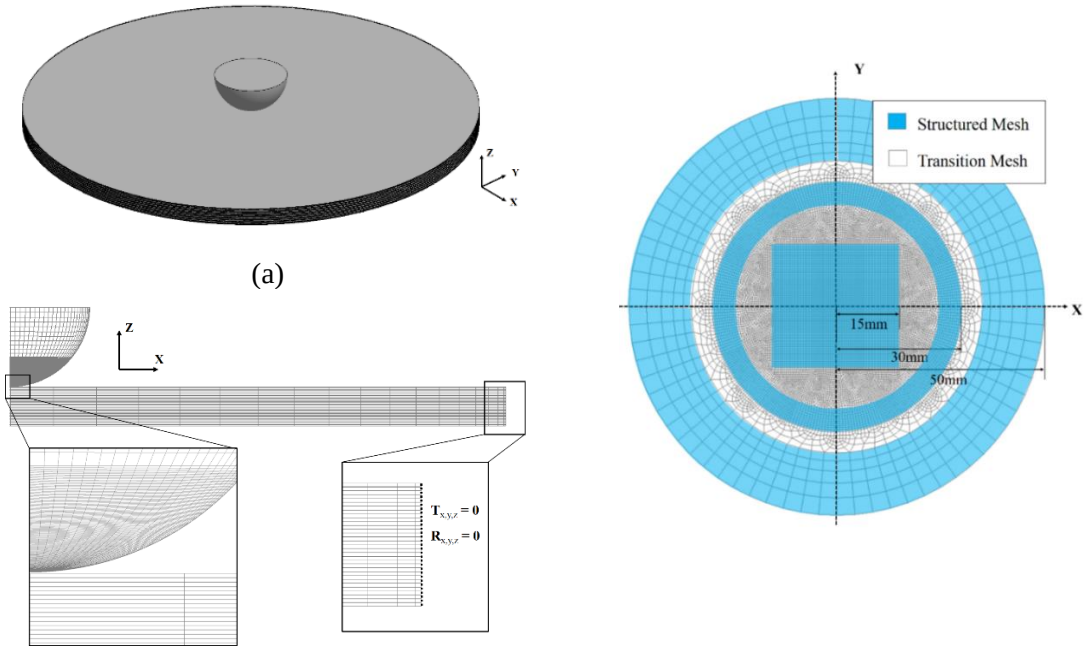

Figure 1: (a) three-dimensional overview of the impact model; (b) Detailed axisymmetric view of the impact model, the left zoom-in view shows position between impactor and laminate model and the right zoom-in view shows the boundary condition of peripheral nodes of the laminate; (c) In-plane mesh distribution of both plies and cohesive layers.

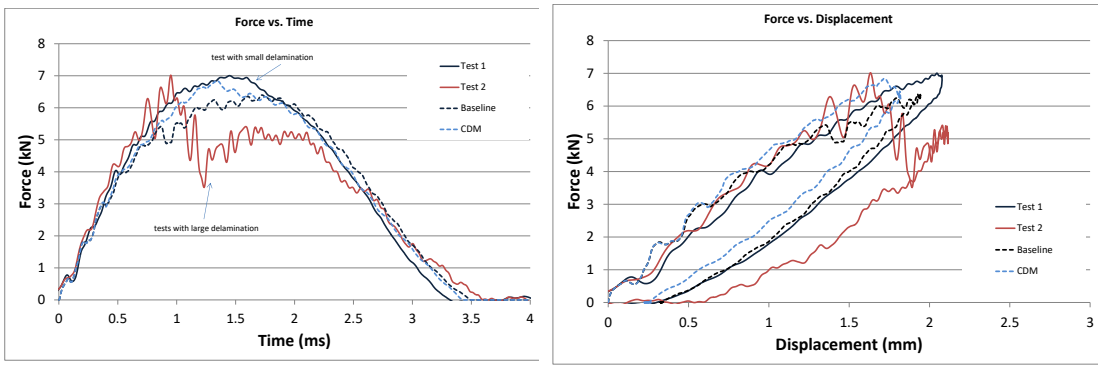

(a) (b)

(c)

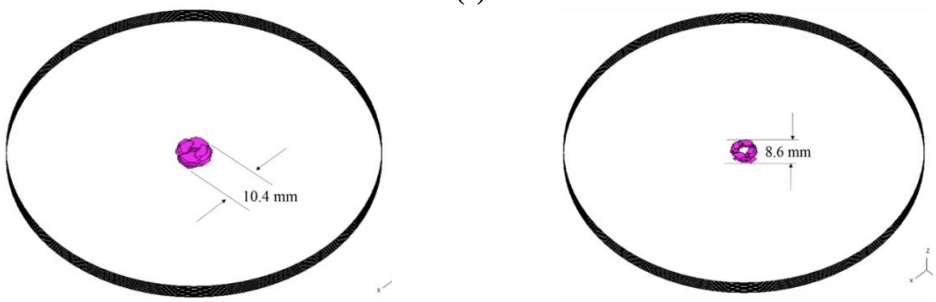

(d) (e)

Figure 2: (a) and (b) showing a comparison between measured and predicted load history s and force displacement curves for the IM7/PEEK material under 8 J impact, (c) C-scanned specimens with damage shape, (d) and (e) predicted delamination size predicted by baseline and CDM models. Note that the outer diameter in (c), (d) and (e) is 100 mm.

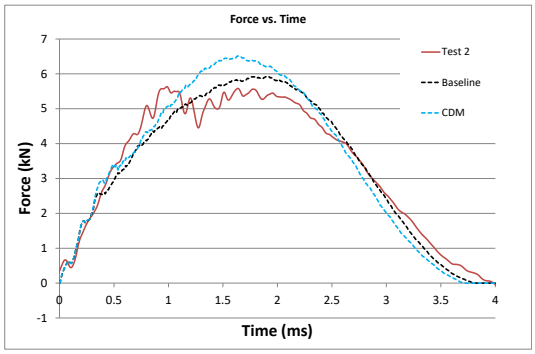

(a)

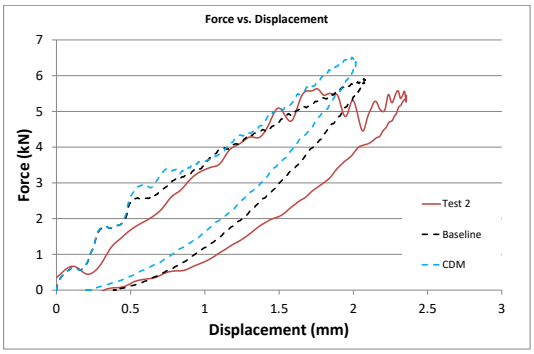

(b)

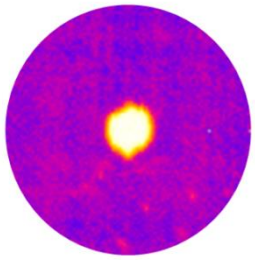

(c)

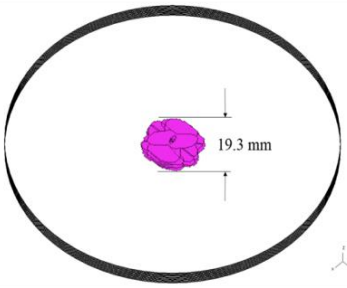

(d)

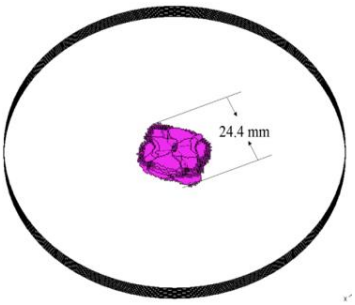

(e)

Figure 3 (a) and (b) showing comparison between measured and predicted load history s and force displacement curves for the IMS65/MTM material under 8 J impact, (c) C-scanned specimen with damage shape, (d) and (e) predicted delamination size predicted by baseline and CDM models, respectively. Note that the outer diameter in (c), (d) and (e) is 100 mm

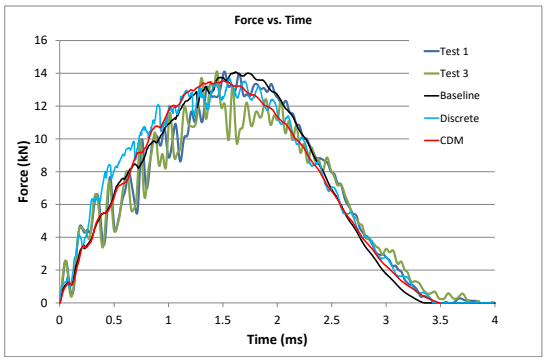

(a)

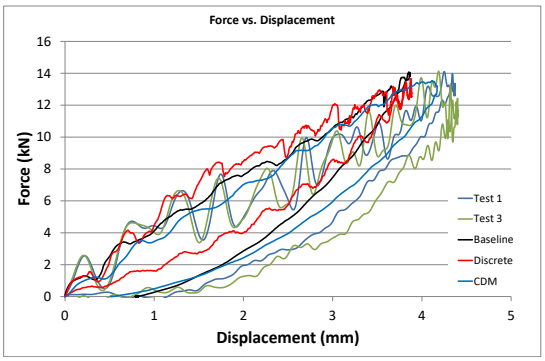

(b)

(c)

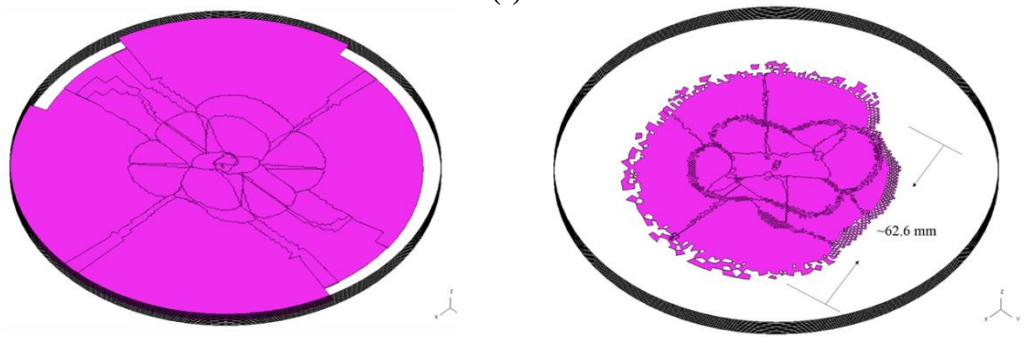

(d) (e)

Figure 4 (a) and (b) showing a comparison between measured and predicted load history s and force displacement curves for the IM7/PEEK material under 30 J impact, (c) C-scanned specimens with damage shape for samples 1 and 3, (d) and (e) predicted delamination size predicted by baseline and CDM models. Note that the outer diameter in (c), (d) and (e) is 100 mm

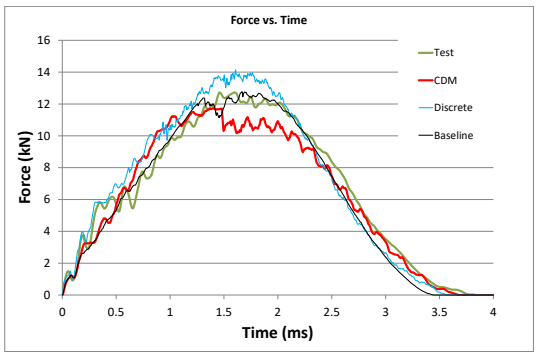

(a)

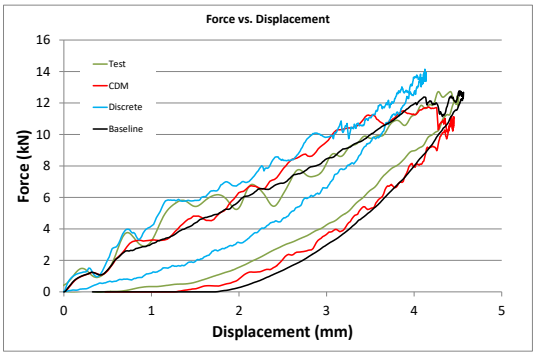

(b)

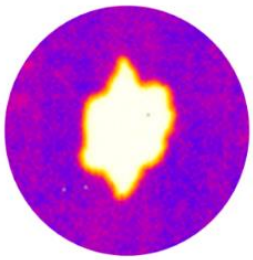

(c)

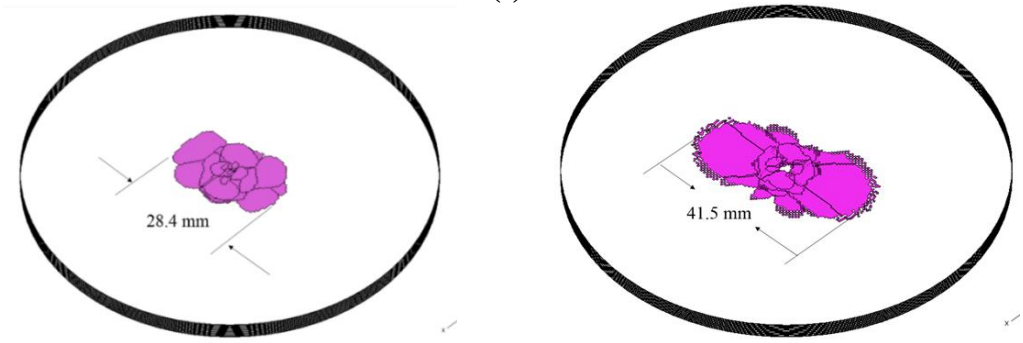

(d) (e)

Figure 5 (a) and (b) showing a comparison between measured and predicted load history s and force displacement curves for the IMS65/MTM material under 30 J impact, (c) C-scanned specimen with damage shape, (d) and (e) predicted delamination size predicted by baseline and CDM models, respectively. Note that the outer diameter in (c), (d) and (e) is 100 mm

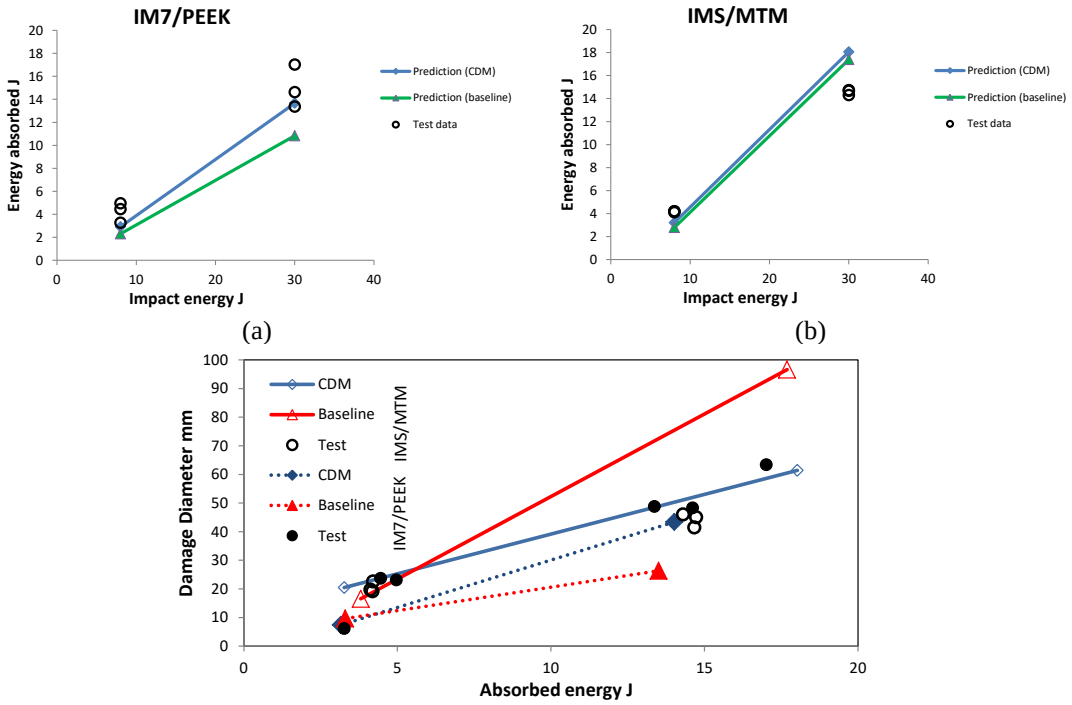

Figure 6 Comparison between measured and predicted results for maximum energy absorbed for (a) IM7/PEEK and (b) IMS65/MTM materials. (c) Variation of the average damage diameter with absorbed energy for the IM7/PEEK and IMS65/MTM panels.

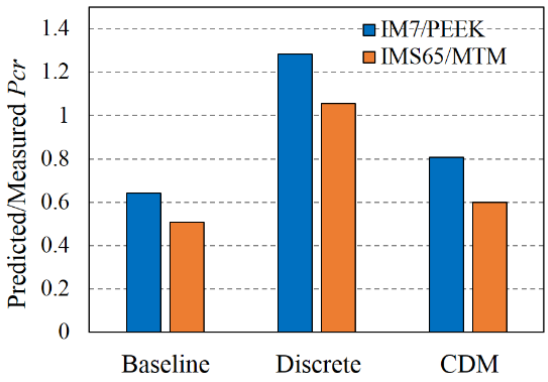

Figure 7: Comparison of normalised critical load (P_{cr}) for both materials under 30J impact.

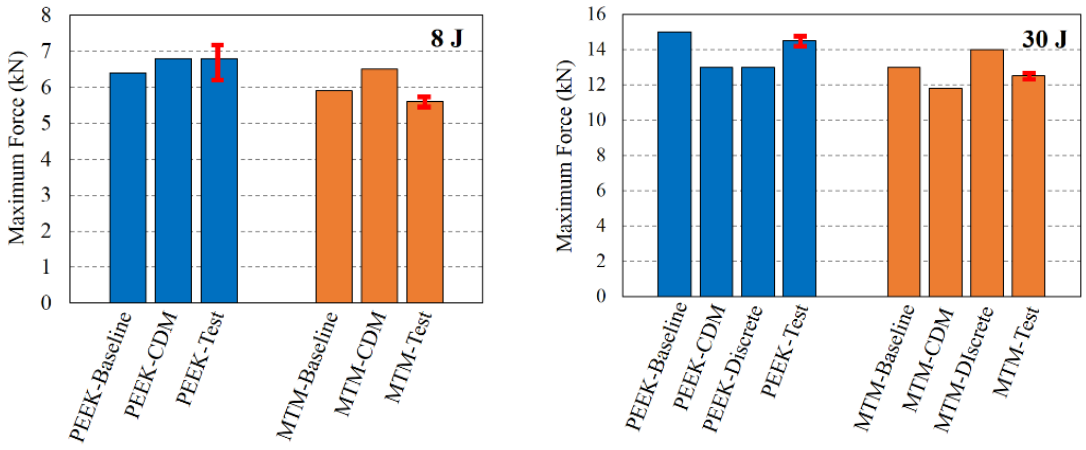

(a) (b)

Figure 8: Comparison between the predicted and measured maximum impact load for IM7/PEEK and IMS65/MTM laminates at 8 and 30J.

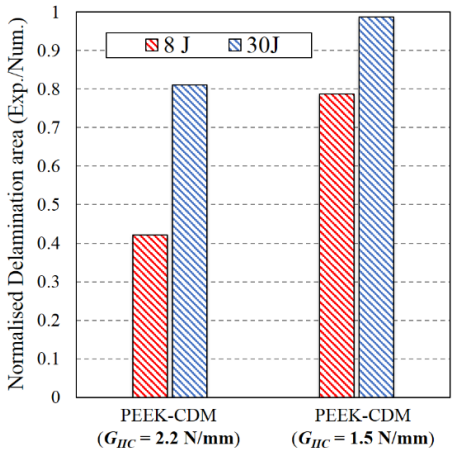

Figure 9 Comparison of predicted delamination of IM7/PEEK under 8 J and 30 J impact simulations using two different G_{IIC} values.

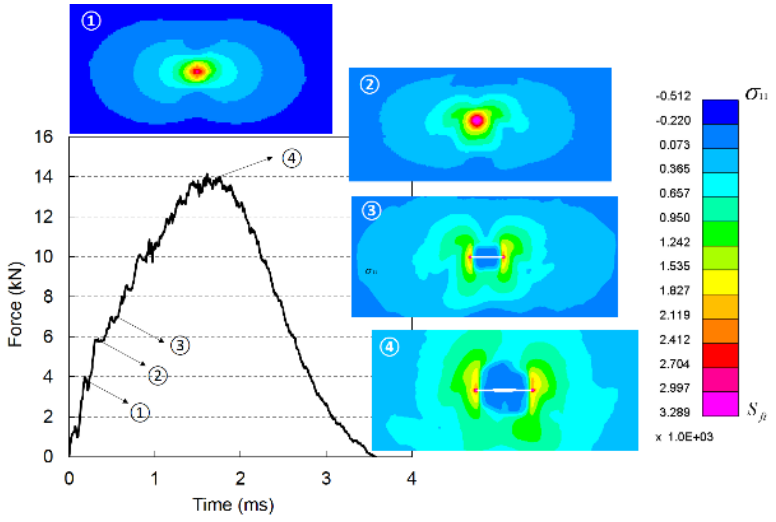

(a)

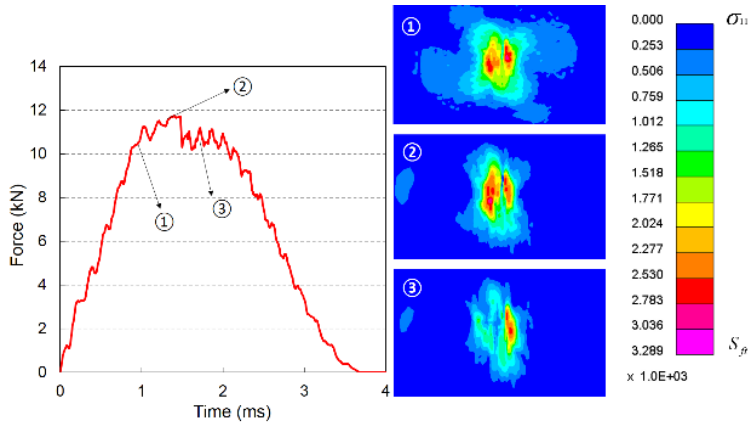

(b)

Figure 10: Progression of fibre direction stress at bottom ply of (a) discrete model and (b) CDM model during impact simulation for IMS65/MTM material at 30 J impact.

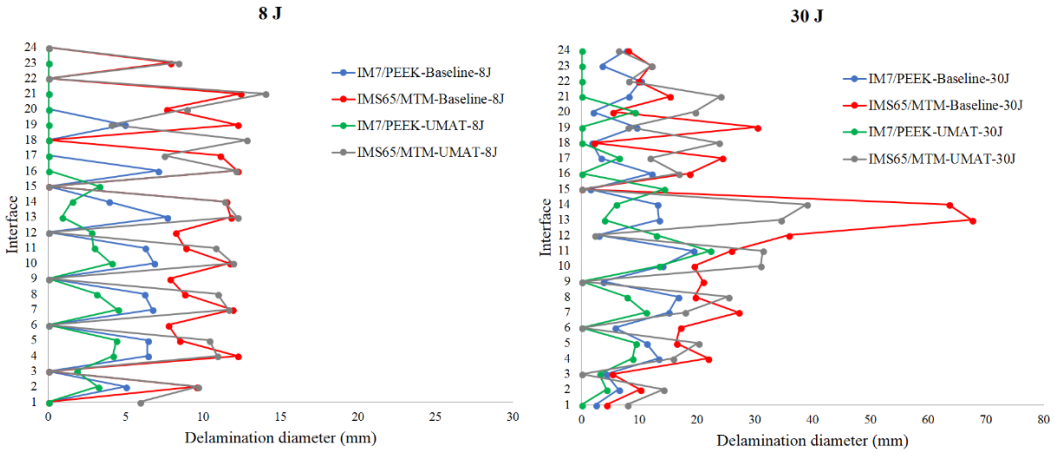

(a) (b)

Figure 11: Distribution of predicted delamination along the interfaces of the IM7/PEEK and IMS65/MTM panels under (a) 8 J and (b) 30 J impact energy, using the Baseline and CDM (UMAT) models.